

The spatial self-organization within pluripotent stem cell colonies is continued in detaching aggregates

Mohamed H. Elsafi Mabrouk^{a,b,*}, Roman Goetzke^{a,b}, Giulio Abagnale^c, Burcu Yesilyurt^d, Lucia Salz^{a,b}, Olivia Cypris^{a,b}, Philipp Glöck^{a,b}, Sven Liesenfelder^{a,b}, Kira Zeevaert^{a,b}, Zhiyao Ma^b, Marcelo A.S. Toledo^e, Ronghui Li^f, Ivan G. Costa^f, Angelika Lampert^g, Vivek Pachauri^h, Uwe Schnakenberg^h, Martin Zenke^{a,b}, Wolfgang Wagner^{a,b,*}

^a Helmholtz-Institute for Biomedical Engineering, Stem Cell Biology and Cellular Engineering, RWTH Aachen University Medical School, Aachen, 52074, Germany

^b Institute for Biomedical Engineering – Cell Biology, RWTH Aachen University Medical School, Aachen, 52074, Germany

^c St. Anna Children's Cancer Research Institute (CCRI), Zimmermannplatz 10, 1090, Vienna, Austria

^d Institute of Pathology, RWTH Aachen University Medical School, Pauwelsstraße 30, 52074, Aachen, Germany

^e Department of Hematology, Oncology, Hemostaseology and Stem Cell Transplantation, Faculty of Medicine, RWTH Aachen University, Aachen, 52074, Germany

^f Institute for Computational Genomics, RWTH Aachen University Medical School, Pauwelsstraße 19, 52074, Aachen, Germany

^g Institute of Physiology, RWTH Aachen University Medical School, Pauwelsstraße 30, 52074, Aachen, Germany

^h Institute of Materials in Electrical Engineering 1 and Chair of Micro-and Nanosystems, RWTH Aachen University, Aachen, 52074, Germany

ARTICLE INFO

Keywords:

Heterogeneity
Pluripotent stem cells
Self-organization
Micro-contact printing
EB formation
Single-cell RNA-Sequencing

ABSTRACT

Colonies of induced pluripotent stem cells (iPSCs) reveal aspects of self-organization even under culture conditions that maintain pluripotency. To investigate the dynamics of this process under spatial confinement, we used either polydimethylsiloxane (PDMS) pillars or micro-contact printing of vitronectin. There was a progressive upregulation of OCT4, E-cadherin, and NANOG within 70 μm from the outer rim of iPSC colonies. Single-cell RNA-sequencing and spatial reconstruction of gene expression demonstrated that OCT4^{high} subsets, residing at the edge of the colony, have pronounced up-regulation of the TGF- β pathway, particularly of NODAL and its inhibitor LEFTY. Interestingly, after 5–7 days, iPSC colonies detached spontaneously from micro-contact printed substrates to form 3D aggregates. This new method allowed generation of embryoid bodies (EBs) of controlled size without enzymatic or mechanical treatment. Within the early 3D aggregates, radial organization and differential gene expression continued in analogy to the changes observed during self-organization of iPSC colonies. Early self-detached aggregates revealed up-regulated germline-specific gene expression patterns as compared to conventional EBs. However, there were no marked differences after further directed differentiation toward hematopoietic, mesenchymal, and neuronal lineages. Our results provide further insight into the gradual self-organization within iPSC colonies and at their transition into EBs.

1. Introduction

Colonies of pluripotent stem cells (PSCs) are not homogeneous but comprise subpopulations that express different levels of pluripotency markers [1–3]. These states are interconvertible: when isolated and re-plated, all subpopulations re-express the whole spectrum of pluripotency markers found in the original culture [4,5]. Higher expression of pluripotency markers is often observed in the subpopulation localized at the border of colonies, which coincides with higher capacity of colony

formation and self-renewal ability [6,7]. This was consistently observed with various approaches for spatial confinement to control the size and shape of PSC colonies [8].

The self-organization within PSC colonies may recapitulate some aspects of early embryogenesis, but the underlying mechanisms and dynamics are not sufficiently understood. Various models have been proposed for this self-organization, including i) differential activation of the transforming growth factor beta (TGF- β) pathway between colony edge and center [7], which might be modulated by Yes-associated

* Corresponding authors. Helmholtz-Institute for Biomedical Engineering, Stem Cell Biology and Cellular Engineering, RWTH Aachen University Medical School, Aachen, 52074, Germany.

E-mail address: mmabrouk@ukaachen.de (M.H. Elsafi Mabrouk).

<https://doi.org/10.1016/j.biomaterials.2022.121389>

Received 28 September 2021; Received in revised form 13 December 2021; Accepted 23 January 2022

Available online 25 January 2022

0142-9612/© 2022 The Authors. Published by Elsevier Ltd. This is an open access article under the CC BY license (<http://creativecommons.org/licenses/by/4.0/>).

protein (YAP) and Transcriptional coactivator with PDZ binding motif (TAZ) activity [9,10], ii) inaccessibility of receptors at the center of the colony [11,12], or iii) a Turing pattern with reaction-diffusion of activators and inhibitors [13]. So far, it is unclear how the spatial heterogeneity within colonies is reflected in transcriptomes of individual cells, or upon transition to three-dimensional organization (3D) towards embryoid bodies (EBs). In addition, it remains a challenge to study the effect of spatial self-organization on the differentiation of PSCs due to the difficulty of controlling other factors affecting iPSCs differentiation, like colony size [14]. In this study, we investigated the dynamics of self-organization of induced pluripotent stem cells (iPSCs) in spatially confined two-dimensional (2D) colonies, self-detached 3D aggregates, and the effect of self-organization on the differentiation biases of early EBs.

2. Materials and methods

2.1. Cell culture of induced pluripotent stem cells

Seven human induced pluripotent stem cell (iPSC) lines were generated from mesenchymal stromal cells (iPSC-102, iPSC-104, and iPSC-106) [15], bone marrow aspirate (iPSC-3-11) [15,16], blood (PT4-WT4, P15-WT108) [17], or human dermal fibroblasts (C2.3) [18] by reprogramming with episomal plasmids or sendai virus. The study was approved by the local ethic committee and all samples were taken after written consent (EK206/09). The iPSC lines were cultured on tissue culture plastic coated with vitronectin (0.5 $\mu\text{g}/\text{cm}^2$) in StemMACS iPS-Brew XF (Miltenyi Biotec). Pluripotency was validated by three lineage differentiation potential and Epi-Pluri-Score analysis, as described in our previous work [19]. Cell counting was done in a Neubauer chamber with trypan blue staining. To analyze viability of non-adherent cells, the floating cells were collected after 24 h after seeding and labeled with fluorescein diacetate (FDA; Sigma) and DAPI. For intermittent calcium depletion, cell culture medium was aspirated and iPSCs were incubated in 2 mM EGTA (Carl Roth) solution in PBS for 20 min followed by incubation in culture medium containing Y-27632 ROCK inhibitor (Abcam). Control samples received knockout DMEM (Gibco) for the same amount of time.

2.2. Generation of PDMS pillars

To fabricate an array of PDMS pillars a photomask was manufactured with circular (diameter of 400, 600, 800 μm) and elliptical features (800 \times 200 μm , 1200 \times 300 μm , 1600 \times 400 μm). The patterns were transferred to a silicon substrate using photolithography and were used as a replication mold. PDMS pillars were then constructed using Sylgard 184 (Dow Chemical Company). Pre-polymer and crosslinking agent were mixed at 9:1 ratio, poured over the silicon master, degassed, and cured for 2 h at 60 °C. Patterned PDMS were then gently peeled-off from the replication mold and were stored in a sealed container until used.

2.3. Micro-contact printing

Micro-contact printing (μCP) was carried out to generate circular adhesion islands with different diameters that facilitate attachment of iPSCs. PDMS pillars were coated with either vitronectin (10 $\mu\text{g}/\text{mL}$), matrigel (100 $\mu\text{g}/\text{mL}$), or laminin (10 $\mu\text{g}/\text{mL}$) for 45 min and then used as stamps on pretreated substrates. For quality control, we alternatively used fluorescently labeled gelatin (Molecular probes). Substrates (either tissue culture plastic or glass) were treated with air plasma (50 W, 1 min). Stamps were brought into conformal contact with the substrate for at least 1 min. Patterned substrates were treated using penicillin/streptomycin solution 1:100 overnight, dried, and stored until use. Cells were seeded at 10,000 cells/ cm^2 .

2.4. Embryoid body formation and differentiation

To form conventional EBs, 80% confluent iPSCs were harvested with collagenase IV (Gibco) for 45 min and transferred to ultra-low attachment plates (Corning). To form spin-EBs, iPSC colonies were treated with Accutase (STEMCELL Technologies) to form single cells. 3,000 cells were dispensed to each well of U-bottom 96 well plates, centrifuged for 6 min at 250 RPM, EBs were harvested 24–48 h after centrifugation and this was considered as day 0 for further differentiation steps. In contrast, our self-detaching EBs formed spontaneously from vitronectin-coated micro-contact printed substrates after 6–8 days in culture. When more than 50% of the colonies detached, aggregates were harvested and considered as day 0 for further differentiation steps. Automatic generation of self-detaching EBs was performed on a liquid handling platform (Hamilton Microlab STAR, Hamilton company). Flushing points were determined using whole-well imaging to collect the self-detached colonies.

Multilineage differentiation of EBs was performed with differentiation induction medium (EB-medium) containing Knockout DMEM (Gibco), 20% FCS (Lonza), 2 mM L-Glutamine, 1x Non-Essential Amino acids, 100 nM β -Mercaptoethanol, and 100 U/mL Penicillin/Streptomycin solution. EBs were differentiated in ultra-low attachment plates for 7 days and harvested at different intervals.

Hematopoietic differentiation was carried out as described before [20]. Briefly, EBs were incubated in EB-medium in ultra-low attachment plates for 5 days followed by incubation in hematopoietic differentiation medium on gelatin-coated plates with regular medium changes for up to 10 weeks. Hematopoietic progenitors were collected regularly starting from week 3. The cells were analyzed by cytopins (stained using Diff-Quik) and by flow cytometry as indicated below. Colony forming unit (CFU) assays were performed by seeding 5,000 hematopoietic progenitors in 500 μL methylcellulose based medium (HSC-CFU lite with EPO; Miltenyi Biotec) in 24-well plates. Colonies were scored after two weeks of culture.

Differentiation toward mesenchymal stromal cells (iMSCs) was carried out using human platelet lysate (HPL) as described before [21]. Medium for self-detaching EBs, spin-EBs, or single cells was changed to MSCs differentiation medium containing 10% HPL. Cells were cultured on 0.1% gelatin coated plates for 35 days. Resulting cells were characterized using flow cytometry and differentiated into osteogenic and adipogenic lineages as described previously [22]. Calcium deposition and fat droplet formation was stained with Alizarin Red and BODIPY, respectively.

Neurosphere differentiation of EBs was carried out according to protocol by Chandrasekaran et al. [23]. EBs were incubated in neural induction medium containing TGF- β and BMP4 inhibitors for 10 days in ultra-low attachment plates. Neurospheres were characterized using flow cytometry using Tuj 1 antibody (BD Bioscience), immunofluorescence, and semi-quantitative reverse-transcriptase PCR (qRT-PCR).

2.5. Immunofluorescence

For immunofluorescence analysis of 2D iPSCs colonies, the cells were fixed with paraformaldehyde (PFA) 4% for 10 min, permeabilized with 0.1% Triton X-100 (Carl Roth) for 10 min, and blocked using 2% bovine serum albumin (BSA) for 30 min. Samples were incubated overnight at 4 °C with primary antibodies against OCT3/4 (clone: H-134), PAX6 (clone: D-10), and N-Cadherin (Clone: H-63; all from Santa-Cruz); NANOG (clone: NNG-811), YAP (clone: EP1674Y), and TAZ (all from Abcam); NODAL (Clone: 5C3; Sigma-Aldrich); LEFTY (R&D systems). Secondary antibody staining was done at room temperature for 1–3 h with donkey anti-goat (Alexa Fluor 488), goat anti-rabbit (Alexa Fluor 594), goat anti-rabbit (Alexa Fluor 647), goat anti-mouse (Alexa Fluor 594), and goat anti-mouse (Alexa Fluor 647); all from Invitrogen. Samples were counterstained with Hoechst 33342 for 10–15 min.

The staining of 3D aggregates was done as described before [24]: 3D

aggregates were fixed using 4% PFA for 1 h followed by permeabilization in 0.1% Triton-X 100 and 0.2% BSA (Sigma-Aldrich). Samples were then stained with primary antibody for PAX6; GATA-6 (clone: D61E4), TUJ-1 (clone: D71G9; both from Cell Signaling); Nestin (clone: 10C2; Sigma-Aldrich); OCT4, NODAL, and LEFTY for 2 days at 4 °C. Secondary antibody staining was carried out for additional 2 days and finally the aggregates were counterstained with Hoechst 33342 for 2 h. Stained samples were embedded in glycerol-fructose clearing solution and mounted employing a spacer between a coverslip and a glass slide. All samples were imaged using LSM 700 confocal microscopy (Carl Zeiss) using 20x and 63× oil-immersion objective with 2× line averaging or EVOS FL (Thermo Fisher) at 4x, 10x, and 20x. Neurospheres were imaged using Olympus Fluoview FV1000 two-photon microscope using 35× water-immersion objective. Radial profile of immunofluorescence images of 2D colonies were quantified using radial profile extended ImageJ plugin [25] and plotted using a custom python script.

2.6. Single cell RNA sequencing and spatial reconstruction of gene expression

Single cell RNA sequencing (scRNA-seq) was performed with the chromium single-cell gene expression platform (10x Genomics). To this end, we used two iPSC lines that were either geometrically confined at day 5, or within self-detached iPSCs aggregates at day 8 after cell seeding. Colonies and aggregates were treated with Accutase for 15 min and sequencing libraries were prepared according to manufacturer's recommended protocol. Sequencing was done with the Illumina NextSeq 500 platform and analyzed using Cell Ranger (10x genomics) and the Seurat R package [26]. Quality control of the data was verified using the number of features. After the exclusion of cells with abnormally high/low number of features, at least 6,000 cells per replica were further analyzed. After filtration, average number of features ranged between 2,400 and 3,000 features per cell; average reads were 8,000–10,000 reads per cell. According to the *POU5F1* (*OCT4*) expression, we classified the top 1,000 cells as *OCT4*^{high} and lowest 1,000 cells as *OCT4*^{low}. Differential gene expression between these groups was carried out using Seurat wrapper for MAST R package (adjusted *P* of <0.05 and a threshold of > ln1.5 was considered significant) [27]. Gene Set Enrichment Analysis was done using ClusterProfiler R package employing fgsea algorithm and gene ontology database [28]. Cell-cycle scoring was carried using the CellCycleScoring module of the Seurat package based on a list of cell marker genes.

Spatial reconstruction of sc-RNA-seq data was carried out using novoSpaRc python package [29]. Normalized gene expression matrices of all non-excluded cells were compensated for drop-out events using ARLA [30]. The reconstruction was carried out using immunofluorescence images of OCT4, NANOG, and E-Cadherin as guidance markers. Images of 600 μm colonies were used to generate the spatial mesh and the reconstruction was performed with alpha value of 0.7 for the marker genes. Pathway enrichment was carried out for subpopulations using the expression profiles of the top 500 pathway responsive genes employing the PROGENy package for scRNA-seq [31,32]. Pathway enrichment was carried out for single cells and averaged for each subpopulation.

2.7. Bulk RNA sequencing

RNA was isolated from either spin-EBs or self-detaching EBs during multilineage differentiation of EBs at day 0, day 3, and day 7 using Nucleospin RNA kit (Macherey-Nagel). Quality control was done with a NanoDrop Spectrophotometer (Thermo Scientific, Wilmington, USA). Library preparation (QuantSeq 3'-mRNA) and sequencing was performed by Life&Brain (Bonn, Germany) on a NovaSeq 6000 sequencer (100 bp/read). Adapter sequences and low quality reads was trimmed using BBDuk, pseudo-alignment and abundance estimation was done using Salmon [33]. Differential expression analysis between spin-EBs and self-detaching EBs was carried out using DESeq2 using Wald test

(adjusted *P* of <0.05 and a threshold of > 2-fold change was considered significant) [34]. Pathway enrichment was performed as described previously using the expression profile of the top 100 pathway responsive genes with the PROGENy package for bulk RNA-seq [31]. Significant pathways for differentiation were identified by comparing the enrichment score of day 0 versus day 3 and day 7 EB samples. Z-scores (normalized to all day 0 samples of μCP-EB and spin-EBs) were compared using paired student t-test for each time point.

2.8. Semi-quantitative reverse-transcriptase PCR

Total RNA was isolated from EBs using Nucleospin RNA kit (Macherey-Nagel) and converted into cDNA using the high capacity cDNA reverse transcription kit (Life Technologies GmbH). Semi-Quantitative PCR (qPCR) was carried out using SYBR green reagent (Applied Biosystems). Primers for neural markers (*TUBB3*, *MAP2*, *GFAP*, and *PAX6*), signaling markers (*ID2*, *MYC*, and *HES5*) and housekeeping gene (*GAPDH*) are provided in Suppl. Table S1.

2.9. Flow cytometry

Cells were dissociated using TrypLE and re-suspended in FACS buffer (1% FCS + 0.4% EDTA). 250,000 cells were stained per panel with antibodies for CD14 (clone: M5E2), CD31 (clone: WM59), CD34 (clone: 581), CD43 (clone: 1G10), CD90 (clone: 5E10), CD73 (clone: AD2), CD29 (clone: MAR4), all BD Bioscience; CD33 (clone: AC104.3E3), CD45 (clone: REA747), CD66b (clone: REA306) from Miltenyi Biotech; KIT (clone: 104D2), CD235a (clone: HIR2) from eBioscience; and CD105 (clone: MEM-226) from immunotools. Flow cytometry was carried out using a FACS Canto II (BD biosciences). Data was further processed using FlowJo (FlowJo LLC).

3. Results

3.1. Progressive self-organization of pluripotency factors in confined colonies

Colonies of iPSCs revealed marked up-regulation of OCT4, E-cadherin, and NANOG at their outer rim region when cultured for six days, e.g. on flat polydimethylsiloxane (PDMS; Fig. 1A). To systematically investigate the impact of culture time and colony size on this self-organization, we utilized circular PDMS micro-pillars of 200 μm height with diameters of 400, 600, and 800 μm (Suppl. Fig. S1A). This setup enables spatially confined cell growth on top of the pillars. Over six days, we observed marked and progressive up-regulation of OCT4, E-cadherin, and NANOG within a ring-shaped region of about 50–70 μm from the colony border, irrespective of pillar size (Fig. 1B). The same increasing up-regulation from the rim was also observed for colonies on elliptical pillars with equivalent growth areas (Suppl. Fig. S1B). Imaging and handling of PDMS micro-pillars was cumbersome and molecular analysis hampered by cell growth between the pillars. Therefore, we alternatively used the array of pillars as a stamp for micro-contact printing (μCP) of the adhesion protein vitronectin on either tissue culture plastic (TCP) or glass substrates (Suppl. Fig. S1C). When iPSCs were seeded on these μCP substrates, their growth was also restricted to circular areas (Suppl. Fig. S1D). In comparison to conventional vitronectin coated TCP, a higher fraction of cells was still non-adherent at 24 h after seeding due to the smaller coated area on the μCP substrates (Suppl. Fig. S2). The adherent cells proliferated under the spatially confined conditions, and we observed a very similar up-regulation of OCT4 and E-cadherin at the outer region as previously observed on the micro-pillars, which was progressive over six days - again within about 50–70 μm distance from the border of the colony (Fig. 1C–D; Suppl. Fig. S1E).

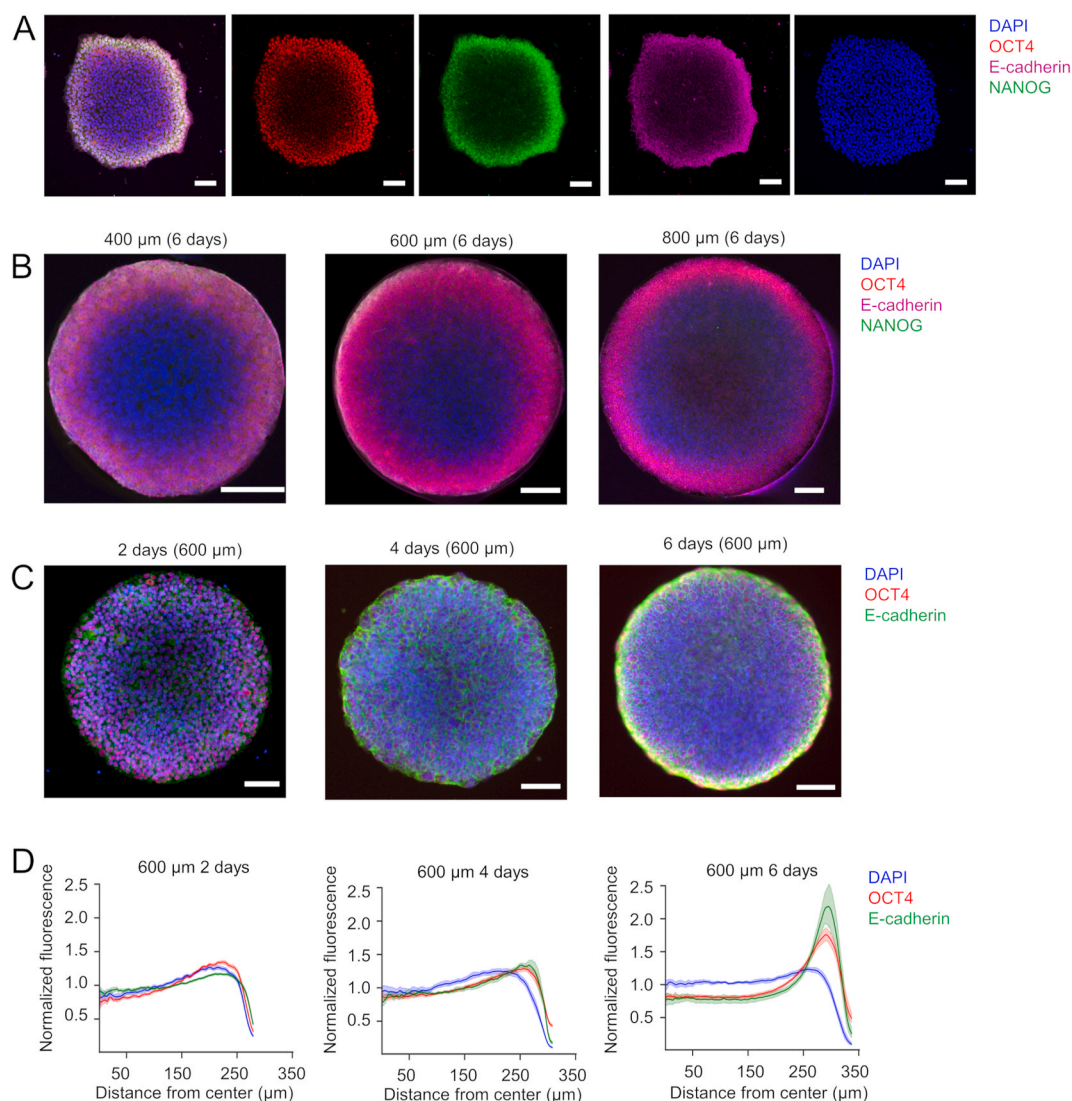


Fig. 1. Spatial self-organization within iPSC colonies.

A) Higher expression of pluripotency markers (OCT4, E-cadherin, and NANOG) is observed at the border regions of induced pluripotent stem cell (iPSC) colonies, which were cultured on flat PDMS substrates for 6 days (scale bar: 50 μm)

B) Up-regulation of NANOG, OCT4, and E-cadherin was particularly observed at the outer region of spatially confined iPSC colonies on PDMS micro-pillars with different diameters (Ø 400 μm, 600 μm, or 800 μm) after 6 days (scale bar: 100 μm)

C) Continuous self-organization was observed on spatially confined iPSC colonies upon micro-contact printing (μCP) of vitronectin on tissue culture plastic (at d2, d4, and d6; scale bar: 100 μm).

D) Quantification of immunofluorescence signals of iPSC colonies on μCP substrates demonstrate progressive organization (in analogy to C; n = 15 per time point).

3.2. Gene expression is heterogeneous in spatially organized colonies

We anticipated that the spatial self-organization within iPSC colonies was also reflected on the transcriptomic level and that this might shed light on the underlying mechanism. Therefore, we performed single-cell RNA sequencing (scRNA-seq) after 5 days of culture on 600 μm diameter μCP substrates using the 10x genomics platform. As a surrogate for the spatial organization of individual cells, we stratified the cells by their *POU5F1* (OCT4) expression level: in t-distributed stochastic neighbor embedding (t-SNE) plots the 1,000 cells with highest and lowest OCT4 expression clustered with a smooth transition (Fig. 2A). The expression pattern of other pluripotency markers (e.g. *NANOG*, *THY1*, and *ZCAN10*) overall matched the expression pattern of OCT4 (Suppl. Fig. S3A). When we directly compared *OCT4*^{high} versus *OCT4*^{low} subpopulations, there were 151 differentially expressed genes (fold change > ln1.5 and adjusted *P* < 0.05; Suppl. Table S2). Interestingly, *NODAL*, *LEFTY1*, and *LEFTY2* were the highest up-regulated genes in the

OCT4^{high} subset (fold-change = 6.2, 5.45, and 4.74, respectively; Fig. 2B). These cytokines of the TGF-β superfamily have important functions in pluripotency maintenance as well as cellular differentiation in early embryogenesis. Similar results were observed with an independent biological replicate of another iPSC-line (Suppl. Figs. S3B and C; Suppl. Table S3). Gene set enrichment analysis (GSEA) revealed that especially genes of the TGF-β signaling pathway are enriched in the *OCT4*^{high} subset (Suppl. Fig. S4A). Interestingly, there was a striking similarity in differential gene expression between the *OCT4*^{high} and *OCT4*^{low} subsets with a recently published study that compared subsets of embryonic stem cells (ESCs) with higher and lower self-renewal capacity (*GCTM2*^{high} *CD9*^{high} *EPCAM*^{high} versus *GCTM2*^{low} *CD9*^{low} *EPCAM*^{low}) [5] (Suppl. Fig. S4B). Pathway enrichment analysis further confirmed upregulation of the TGF-β, WNT, MAPK, and JAK-STAT pathways in the *OCT4*^{high} subpopulation (Suppl. Fig. S4C). Those pathways are involved in regulation of pluripotency maintenance and differentiation of iPSCs [35,36].

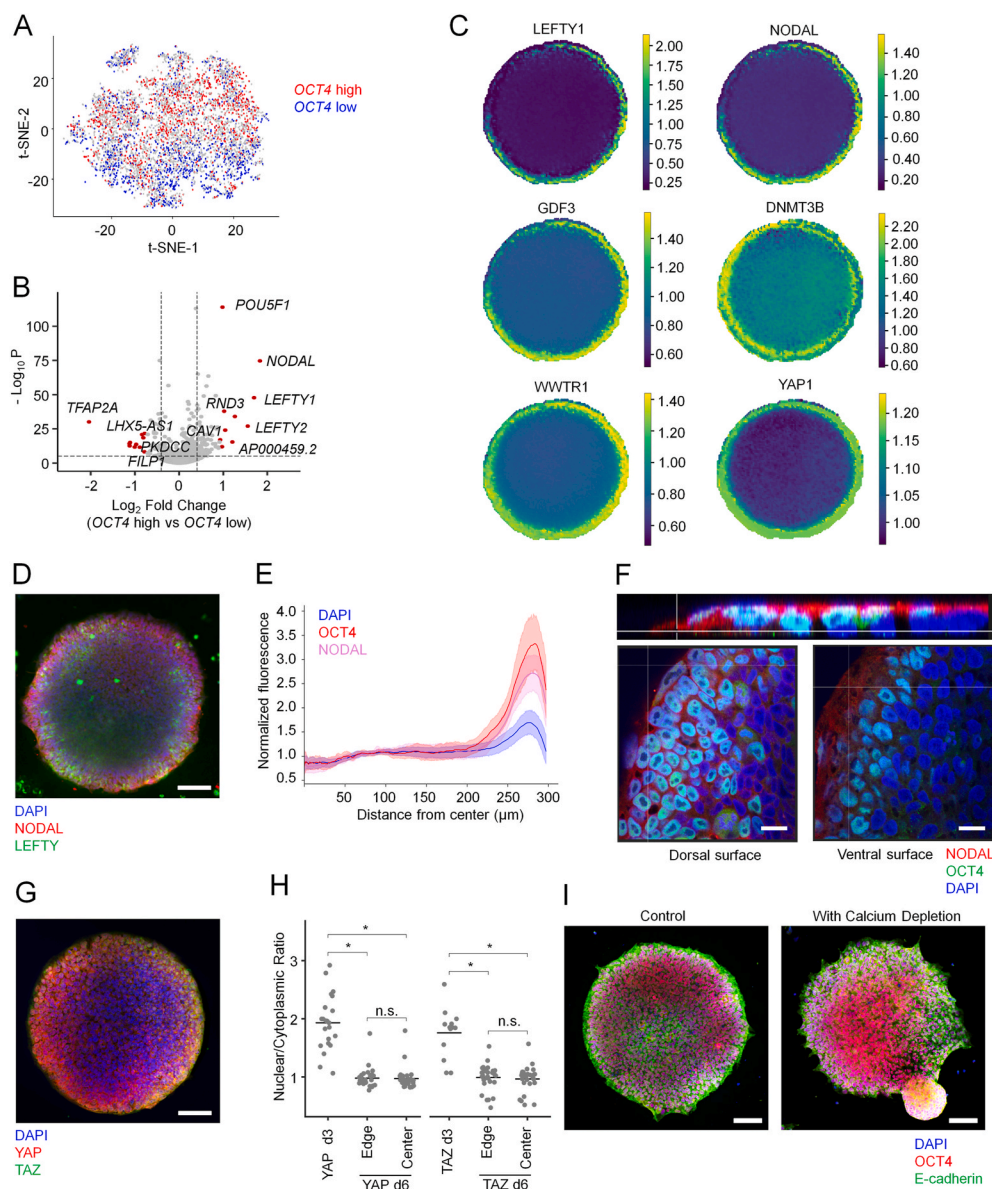


Fig. 2. Relevant parameters for the spatial self-organization of iPSC colonies.

A) Single-cell RNA-sequencing was performed with self-organized iPSC colonies at day 5 on μ CP substrates (\varnothing 600 μ m). The t-SNE plot highlights $OCT4^{high}$ (red) and $OCT4^{low}$ (blue) subfractions.

B) Volcano plot of differential gene expression in $OCT4^{high}$ versus $OCT4^{low}$ subsets demonstrates that *NODAL*, *LEFTY1*, and *LEFTY2* have highest up-regulation in $OCT4^{high}$ subsets.

C) Spatial reconstruction of normalized gene expression for *NODAL* and its inhibitor *LEFTY1*, pluripotency markers *GDF3*, *DNMT3B*, and hippo pathway effectors *YAP1* and *WWTR1* (*TAZ*).

D) Immunofluorescence image of iPSCs at day 6 on μ CP substrate (\varnothing 600 μ m) demonstrates that expression of *NODAL* has similar spatial organization as *OCT4*, whereas *LEFTY* reveals rather patchy expression at the border (scale bar: 100 μ m)

E) Quantification of the radial profile of immunofluorescence signals of *OCT4* and *NODAL* ($n = 20$ colonies).

F) Perpendicular cut of Z-stack of spatially confined colony showing that on the dorsal surface of the colonies there is more expression of *NODAL* compared to the ventral surface of a self-organized colony (day 6 on μ CP substrate; \varnothing 600 μ m; scale bar: 20 μ m)

G) *YAP* and *TAZ* staining of a spatially confined iPSC colony (day 6 on μ CP substrate; \varnothing 600 μ m) demonstrates up-regulation of both proteins at the edge of the colony (scale bar: 100 μ m)

H) Quantification of nuclear/cytoplasmic ratio of *YAP* and *TAZ* within spatially confined colonies at day 3 or day 6 (either center or edge of the colony; on μ CP substrate, \varnothing 600 μ m) demonstrates shift to the nuclear compartment at later time points (12 colonies for d3, 25 colonies for d6; $*P < 0.001$; n. s. = not significant; *t*-test with Bonferroni correction).

I) Immunofluorescence image depicts spatial organization of *OCT4* and *E-cadherin* (on μ CP substrates, \varnothing 600 μ m, d6) without or with intermittent calcium depletion by 2 mM EGTA (for 20 min at d5; scale bar: 50 μ m). (For interpretation of the references to

colour in this figure legend, the reader is referred to the Web version of this article.)

To explore the self-organization of gene expression in other genes, we performed spatial reconstruction of sc-RNA-seq results using immunofluorescence images of *OCT4*, *NANOG*, and *E-Cadherin* for the guiding mesh (Suppl. Fig. S5A). The reconstruction of spatial positions is based on searching for arrangements of the sequenced cells in which nearby cells have transcriptional profiles that are more similar than those farther apart [29]. We exemplarily validated that the reconstruction approach could predict *in silico* the expression pattern for *PAX6* and *CDH2* by immunofluorescence analysis of spatially confined colonies (Suppl. Fig. S5B). Notably, this approach indicated that also several other genes are higher expressed within a ring-shaped region at the colony border, such as *NODAL* and *LEFTY1*, pluripotency markers as *DNMT3B* and *GDF3*, and hippo-pathway effectors *YAP1* and *WWTR1* (*TAZ*) (Fig. 2C). As TGF- β pathway is linked to the self-renewal ability of stem cells, we reconstructed the spatial patterning of cell cycle score using the

expression of canonical cell cycle markers. In fact, the edge of the colony revealed higher average score for the G2/M phases, whereas the center showed higher average G1 score (Suppl. Fig. S5C). Overall, the results suggested that cells in the border region of iPSC colonies are in a more primitive and proliferative state, and that the TGF- β pathway plays a central role for the spatial organization.

We next focused on expression dynamics of *NODAL* and *LEFTY* as they were the most differentially expressed genes. Confocal immunofluorescence analysis of *NODAL* and *LEFTY* showed similar up-regulation at the border region of confined iPSC colonies with continuous progression over six days, similar to the segregation of *OCT4* (Fig. 2D and E). *NODAL* staining was more prominent on the dorsal surface of the colony, particularly at the border (Fig. 2F). We subsequently analyzed expression of *YAP* and *TAZ* that generally play a crucial role for cell-matrix and cell-cell interaction [37]. Both

transcription coactivators were up-regulated at the edge of the colony (Fig. 2G; Suppl. Fig. S6A), which is in line with previous observations [38]. At early time points (at day 3) YAP and TAZ were preferentially localized at nuclear compartment, whereas their localization shifted to the cytoplasm at later time points (day 6; $P < 0.0001$). However, there was no significant difference in the nuclear/cytoplasmic ratio of YAP and TAZ between edge *versus* center of the colony (Fig. 2H).

To address the relevance of calcium dependent cell-cell interaction for segregation of OCT4 and E-cadherin, we used intermittent calcium depletion by treatment with egtazic acid (EGTA) for 20 min at day 5 followed by incubation with rho-associated protein kinase (ROCK) inhibitor-containing medium. Staining of zonula occludens-1 (ZO-1) at day 6 demonstrated that the neither tight-junctions nor adherens junctions were fully re-established after 24 h after calcium chelation (Suppl. Figs. S6B and C). The intermittent calcium depletion in combination with ROCK inhibition - but neither of them individually - abolished the self-organization of OCT4, though not E-cadherin, at the border region of the colonies (Fig. 2I), indicating that cell-cell interaction is relevant for the spatial self-organization.

3.3. Spontaneous formation of 3D aggregates from μ CP substrates

After about one week of culture, most of the iPSC colonies detached spontaneously from μ CP substrates (Fig. 3A; Suppl. Movie S1). While this was initially unintended, we noticed that this detaching worked very consistently without additional enzymatic or mechanical treatment – hence, the method might be applied for generation of early iPSC aggregates. We tested five different iPSC lines and all of them demonstrated reproducible detachment of most colonies within a defined time-window between day 6 and day 8 (Fig. 3B). Within the floating self-detached aggregates, we hardly observed dead cells and they were capable of differentiation into the three germ layers upon induction with FCS-containing medium, in analogy to conventional methods for EB formation (Fig. 3C). The size of these self-detaching EBs (μ CP-EBs) could be modulated by changing the diameter of the μ CP pattern: μ CP areas of 400 μ m diameter gave rise to aggregates of 248.3 ± 40.6 μ m diameter; 800 μ m spots produced aggregates of 362.9 ± 51.1 μ m in diameter (Fig. 3D). For comparison we also generated EBs with enzymatic harvesting of a cell layer, which resulted in a much larger size-distribution (263 ± 140.4 μ m), whereas EB-formation with aggregation of defined

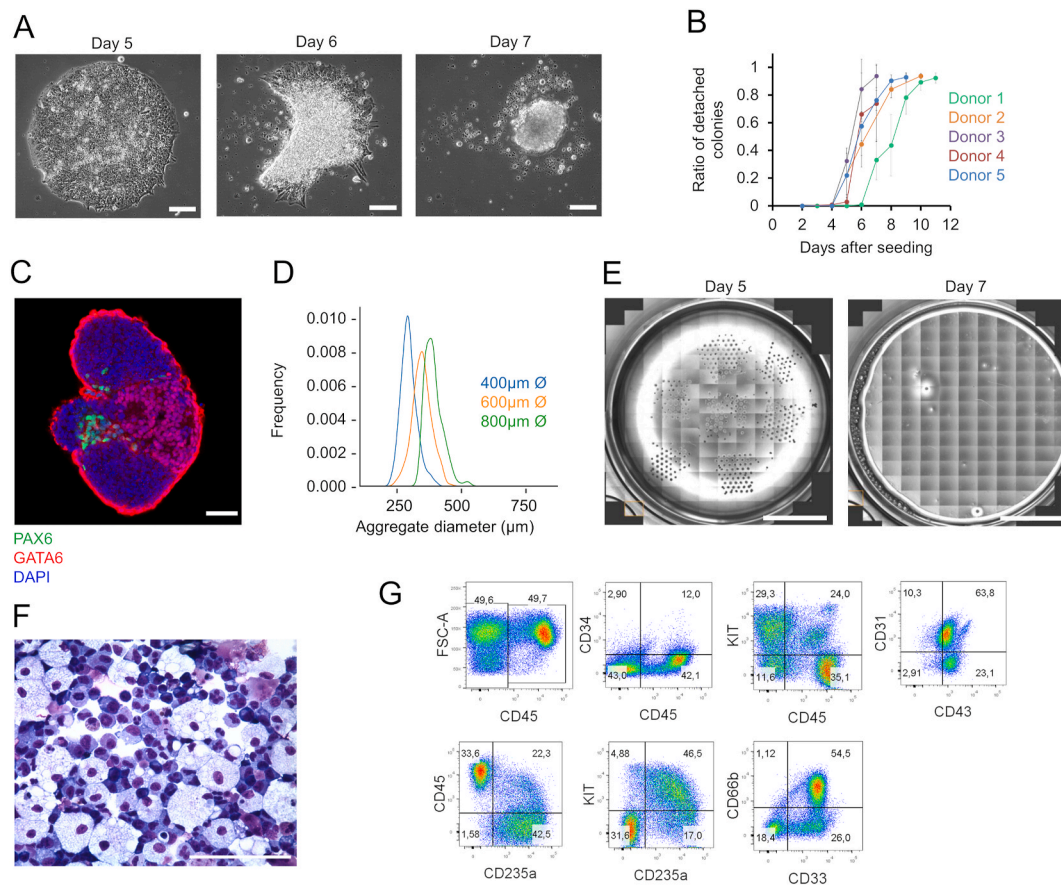


Fig. 3. EBs generated by self-detachment from micro-contact printing substrates.

A) Phase contrast images from a live cell imaging sequence showing the detachment process of a colony from micro-contact printed vitronectin (μ CP; \varnothing 600 μ m) on tissue culture plastic. Confluent colonies at day 5 retracted and finally detached at day 7 after seeding (scale bar: 100 μ m)

B) Kinetics of colony detachment of iPSCs cell lines of five different donors (three replicas for each iPSC lines; \pm standard deviation).

C) Confocal fluorescence microscopic analysis of a self-detached EB after further differentiation in FCS-containing medium for 7 days. PAX6 expression is indicative for neuroectodermal differentiation, whereas GATA6 is expressed in the definitive endoderm and blocks early epiblast differentiation (scale bar: 100 μ m).

D) Histogram of size-distribution of self-detached aggregates generated with μ CP areas of different diameter.

E) Generation of self-detaching EBs using a liquid handling unit. The phase contrast images depict a whole cell culture well with μ CP areas (\varnothing 600 μ m per dot) before (left panel) and after (right panel) the self-detachment process with semiautomated cell culture (scale bar: 10 mm)

F) Cytospin analysis upon hematopoietic differentiation of semi-automatically generated self-detached EBs reveals typical morphology of various types of myeloid cells (stained with Diff-Quik; scale bar: 50 μ m)

G) Flow cytometry demonstrates up-regulation of hematopoietic markers upon hematopoietic differentiation of self-detaching EBs, which were generated semi-automatically using a liquid handling unit.

cell numbers by centrifugation (spin-EBs) resulted in smaller variation in aggregate size (Suppl. Figs. S7A and B).

Supplementary data related to this article can be found at <https://doi.org/10.1016/j.biomaterials.2022.121389>.

To elucidate relevance of coating protein in the self-detachment process we compared μ CP with vitronectin, laminin and matrigel. On laminin-coated surfaces, colonies were able to detach in similar dynamic but less efficient as compared to vitronectin-coated surfaces. On matrigel-coated substrates, there was hardly any colony detached even after 10 days in culture (Suppl. Fig. S7C), indicating that the protein coating is relevant for this process. Subsequently, we analyzed if dried vitronectin μ CP substrates remained functional even after long-term storage, which would ease production, supply, and shipment of μ CP cell culture plates. In fact, growth of iPSCs, geometric conferment, self-organization, and detachment were also observed 90 days after μ CP (Suppl. Fig. S7D).

An advantage of the μ CP-EBs as compared other methods for EB formation is that the processing steps could be easily automated without the need of centrifugation steps or sorting into small multi-well plates. In fact, using a liquid handling unit we could reliably harvest uniform μ CP-EBs (Fig. 3E). These automatically generated self-detaching EBs could also be stimulated for direct differentiation toward hematopoietic lineages in a semiautomatic setting (Fig. 3F and G). Taken together, the self-detachment of iPSC colonies from μ CP substrates provides a powerful approach to generate large numbers of size controlled-EBs without the need of enzymatic or mechanical treatment.

3.4. Self-detaching aggregates maintain aspects of the spatial organization

We subsequently analyzed if the spatial self-organization, which we observed in the 2D colonies, progresses upon transition to 3D. After detaching from the μ CP substrates (1–2 days after detachment of initial colonies), immunofluorescence staining of E-cadherin and OCT4 demonstrated heterogeneity within μ CP-EBs with marked up-regulation at the outer cell layers. In contrast, spin-EBs revealed a much more uniform pattern 1–2 days after aggregation (Fig. 4A). Furthermore, in μ CP-EBs the pattern of NODAL expression was very similar to OCT4, having higher expression at the rim than in the center of the aggregates (Fig. 4B).

To gain insight into the heterogeneity of transcriptional activity within the early μ CP-EBs, we performed scRNA-seq of 3D aggregates at day 8 after seeding of the cells on 600 μ m diameter μ CP substrates (about 1–2 days after self-detaching of aggregates). We compared gene expression of 1,000 cells with highest versus lowest OCT4 expression in analogy to the differential gene expression analysis in the self-organized 2D iPSC colonies. t-SNE dimensional reduction shows that these two populations were separated more clearly to opposite poles of the t-SNE plot (Fig. 4C). 975 genes revealed significant differential expression between $OCT4^{\text{high}}$ and $OCT4^{\text{low}}$ subsets in the aggregates (fold change of $\ln 1.5$ and adjusted $P < 0.05$; Suppl. Table S3). Several members of the NODAL signaling pathway (*LEFTY1*, *TDGF1*, *NODAL*) were again the highest differentially expressed genes between the two subpopulations (Fig. 4D). To better understand if the differential gene expression in the self-organized 2D colonies progressed from day 5 (in the 2D colonies) to

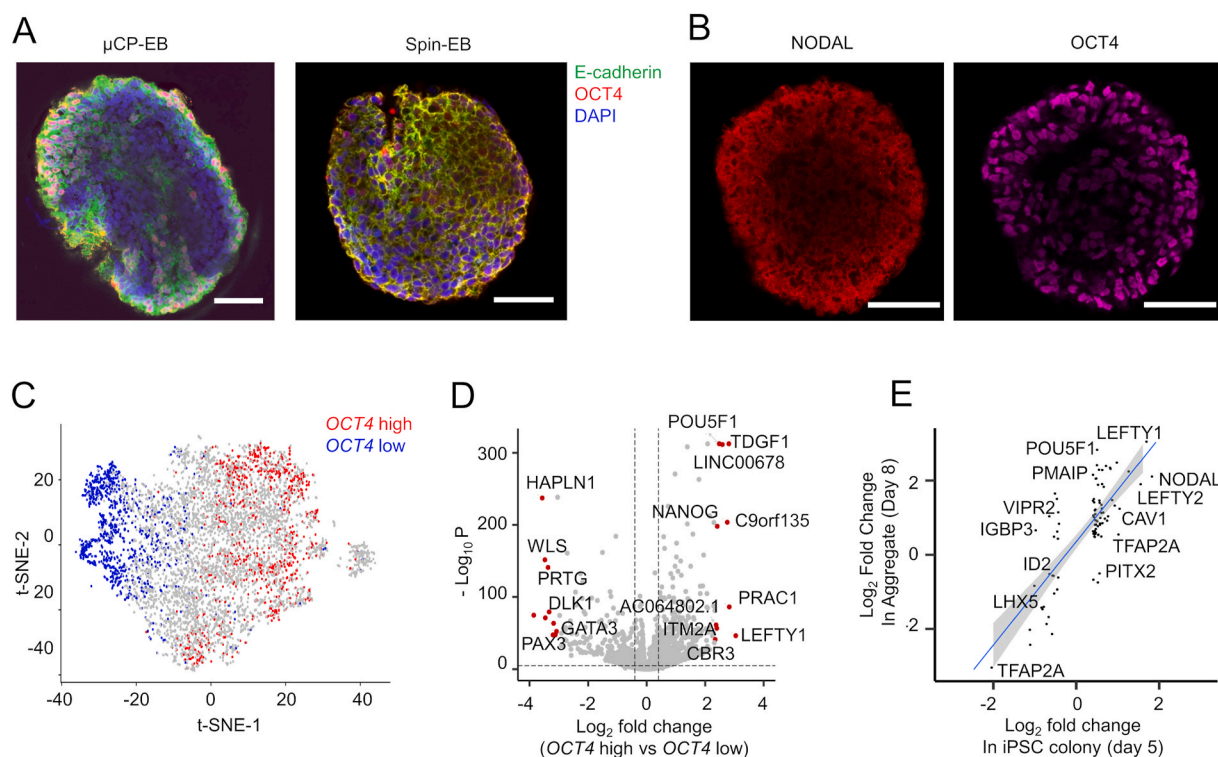


Fig. 4. Self-organization within the self-detached 3D aggregates.

A) Confocal imaging of aggregates generated by self-detachment from micro-contact printed vitronectin (d8 after seeding of iPSCs on μ CP substrates; \varnothing 600 μ m) or pellet formation with centrifugation (spin-EB; after 24 h in the same pluripotency-supporting medium; scale bar: 50 μ m)

B) Confocal imaging of self-detached EB reveals that NODAL and OCT4 are higher expressed at the outer layers (scale bar: 50 μ m)

C) Single-cell RNA-sequencing of early self-detached aggregates (d8 after seeding on μ CP substrates; \varnothing 600 μ m). The t-SNE plot demonstrates further separation of $OCT4^{\text{high}}$ and $OCT4^{\text{low}}$ subpopulations.

D) Volcano plot of differential gene expression between $OCT4^{\text{high}}$ and $OCT4^{\text{low}}$ subsets. *LEFTY1*, *NANOG*, and *TDGF1* (NODAL co-receptor) are amongst the genes with highest differential expression.

E) Comparison of the differential gene expression between $OCT4^{\text{high}}$ and $OCT4^{\text{low}}$ within either self-organized iPSC colonies on μ CP substrates (day 5 after seeding) or upon self-detachment and early aggregate formation (day 8). Genes that were differentially expressed at both time points are indicated ($R^2 = 0.563$, $P < 0.001$).

day 8 (in early μ CP-EBs), we directly compared the fold-changes of $OCT4^{high}/OCT4^{low}$ subsets: overall, the fold changes became even more pronounced in the 3D aggregates at day 8, for both the upregulated and the downregulated genes. Furthermore, genes that were differentially expressed at both time points revealed clear correlation in differential gene expression (Pearson correlation coefficient = 0.755, $P < 0.001$), indicating progression of the transcriptional heterogeneity (Fig. 4E). The results were validated with self-detached aggregates of another iPSC-line (Suppl. Figs. S8A and B). GSEA indicated that particularly mitochondrial genes and genes of metabolic pathways were enriched in the $OCT4^{high}$ subset, whereas various developmental pathways were rather activated in the $OCT4^{low}$ subset (Suppl. Fig. S8C). These results indicate that the cellular specification in the spatially organized 2D iPSC-colonies continues after detaching in the 3D aggregates.

3.5. Self-detached aggregates reveal higher expression of germ layer marker genes

To further analyze if the progressive self-organization in iPSC colonies and self-detached aggregates supports early differentiation steps, we have directly compared expression profiles of un-organized EBs (spin-EBs) and self-detached EBs (μ CP-EBs) during spontaneous germ layer differentiation. Multidimensional scaling (MDS) plot revealed a clear separation of spin-EBs and μ CP-EBs at day 0 (1–2 days after a centrifugation in U-bottom 96 well plates, or 1–2 days after detachment, respectively); however, at day 3 and day 7 both types of EBs clustered closer together with self-detaching EBs showing less heterogeneity at day 3 and day 7 (Fig. 5A; three biological replica per time point and EB

type). The number of significant gene expression differences between spin-EBs and μ CP-EBs (>2 fold change and adjusted $P < 0.05$) did not change substantially during the differentiation course. Many of these genes were related to germ layer differentiation (Fig. 5B). We subsequently analyzed expression of canonical germ-layer related genes and found that μ CP-EBs have particularly higher expression of ectoderm-related genes at day 0, whereas endoderm and mesoderm-related genes are higher expressed at day 3 and day 7 (Fig. 5C).

To gain further insight into the potential mechanisms of early cell-fate decisions in μ CP-EBs and spin-EBs we analyzed pathway enrichment. In comparison to early cell aggregates (D0) particularly the TGF- β , WNT, MAPK, and PI3K pathways were significantly changing during differentiation ($P < 0.05$; Suppl Fig. S9A). Furthermore, at day 0 the TGF- β and WNT pathway activities were significantly higher in μ CP-EBs than in spin-EBs, whereas this was adjusted at later time points (Suppl. Fig. S9B). These results indicate that the 2D self-organization enhances early cell-fate decisions in self-detached aggregates as compared to formation of non-organized spin-EBs and this is probably connected to continued activation of relevant signaling pathways for pluripotency and differentiation.

3.6. Differentiation potential μ CP-EBs versus spin-EBs

Since early 3D aggregates revealed significant differences in germ-layer associated genes in spontaneous differentiation, we investigated if there are also clear functional differences during directed differentiation toward hematopoietic, mesenchymal, or neuronal lineages. Upon hematopoietic differentiation, both EB types gave rise to similar

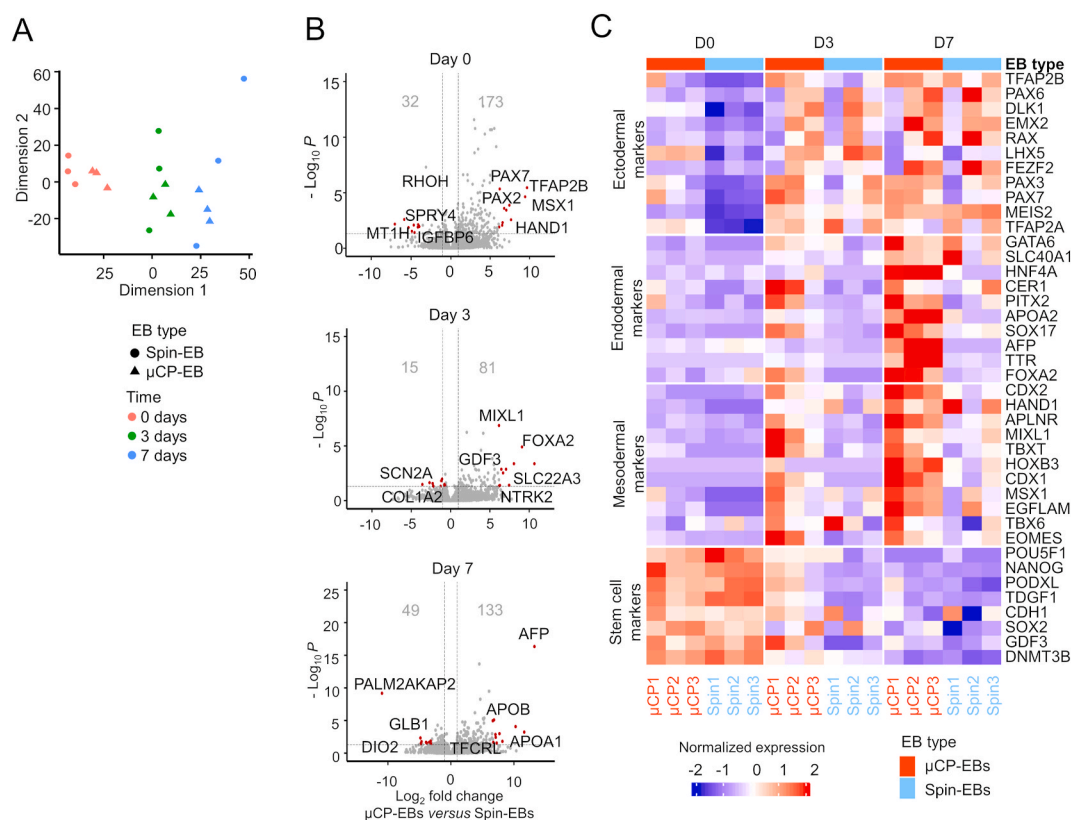


Fig. 5. Differentiation bias of self-organized EBs.

A) Multidimensional scaling (MDS) plot of RNA sequencing data of self-detached aggregates from μ CP substrates (μ CP-EBs) and aggregates of single cells (spin-EBs) during spontaneous differentiation at day 0, day 3, and day 7.

B) Volcano plots showing the differentially expressed genes between μ CP-EBs and spin-EBs at each time point. The number of significant genes is indicated (>2 fold change and adjusted $P < 0.05$; Wald test with Benjamini-Hochberg correction).

C) Heatmap showing the normalized expression level of canonical markers for stem cells plus markers for the three germ layers (gene expression is normalized per row).

numbers of colony forming units (CFUs) in three biological replica. The phenotypic classification of CFUs suggested that μ CP-EBs gave rise to more CFUs of macrophage (CFU-M) and erythroid (CFU-E, BFU-E) appearance, whereas spin-EBs were rather classified as common myeloid progenitor cells (CFU-GEMM) and granulocyte-macrophage progenitors (CFU-GM; Supp. Fig. S10A). However, flow cytometry did not reveal clear differences in hematopoietic progenitor cells derived from either μ CP-EBs or spin-EBs (Supp. Fig. S10B).

Differentiation towards mesenchymal stromal cells (iMSCs) was performed in parallel from single iPSC, spin-EBs, and μ CP-EBs (three biological replica). After 35 days, all iMSCs revealed very similar fibroblastoid cellular morphology and similar differentiation capacity towards adipogenic and osteogenic lineages (Supp. Fig. S11A). Flow cytometric analysis revealed high heterogeneity in surface marker expression, while the typical MSC-markers CD29, CD73, CD90, and CD105 were in tendency slightly higher expressed in iMSCs from μ CP-EBs (Supp. Figs. S11B and C).

When we directed differentiation of spin-EBs and μ CP-EBs into neurospheres we observed a similar fraction of TUJ1+ cells with marked heterogeneity between the three biological replica (Supp. Fig. S12A). This was in line with immunofluorescence staining of TUJ1 and Nestin (Supp. Fig. S12B). Furthermore, gene expression of neuronal marker genes (*TUBB3*, *MAP2*, *GFAP*, *PAX6*, *ID2*, *MYC*, and *HES5*) was also similar in both EB-types with high variation between the replica (Supp. Fig. S12C). Taken together, there was no clear functional difference between μ CP-EBs and spin-EBs upon directed long-term differentiation toward hematopoietic, mesenchymal, and neuronal lineages.

4. Discussion

Pluripotency is maintained and stabilized by a network of pluripotency associated genes as well as by external signals [39]. Previous reports have demonstrated that cells at the edge of PSC colonies have higher expression of pluripotency markers (OCT4, GDF3, Cripto1) as well as higher self-renewal capacity as compared to cells at the colony center [4,6]. Other studies demonstrated that geometric confinement recapitulates the self-organized patterning of human embryonic stem cells (hESCs) [7]. We demonstrate that the spatial self-organization of OCT4 and E-cadherin expressing subsets progresses continuously in geometrically confined iPSCs with culture time. Furthermore, the organization is very similar on PDMS, TCP, and glass, indicating that it is independent of the substrate.

Our single cell gene expression analysis demonstrated that the $OCT4^{high}$ cells, which are typically localized at the border of the self-organized colony, have similar expression patterns to hESCs subsets that display high self-renewal capacity [5]. In addition, pathway enrichment analysis confirmed previous results that the WNT and TGF- β pathways are upregulated at iPSCs colony edge [12,40]. Furthermore, we have also used our scRNA-seq data for gene expression cartography [29]. The predicted spatial reconstruction matched very well with the immunofluorescence images of all genes tested (LEFTY, NODAL, YAP, TAZ, N-cadherin, and PAX6), indicating that our dataset provides an important resource to better understand the spatial distribution of transcriptomes within iPSC colonies.

It was striking that amongst the most differentially expressed genes between $OCT4^{high}$ and $OCT4^{low}$ cells were *NODAL*, *LEFTY*, and other components of TGF- β pathway and they were predicted to be preferentially expressed at the colony edge. Furthermore, disruption of cell-cell interaction resulted in alteration of the self-organization pattern whereas YAP and TAZ transcriptional co-activators showed no preferential activation at the edge and center of the colony. This points to the relevance of the TGF- β and cell-cell interaction in the process of self-organization of geometrically confined PSC colonies, which needs to be further analyzed in the future.

In addition, we describe a new approach to generate EBs from μ CP substrates. This method does not require enzymatic treatment,

dispensing into microwells, or centrifugation steps and can therefore be easily implemented for automated cell-culture regimen. The method worked reliable and facilitated generation of EBs of relatively homogeneous size. Another advantage of μ CP-EBs is its scalability of this approach as compared to traditional EB generation methods: with about 10^6 cells that are seeded into a μ CP 6-well plate format about 3000 μ CP-EBs could be generated simultaneously. To produce similar number of EBs with the spin-EB protocol the starting cell number would be around 10^7 cells distributed across thirty-four 96-well plates. Our results indicate that the dried μ CP plates can be stored for at least three months, indicating that they can be generated in larger batches in a centralized manner or by a distributor. However, the production of μ CP-EBs is less synchronized than other EB-methods as the detachment process takes place over 2–3 days. Therefore, regular assessment of the detachment process is required. Either way, μ CP-EBs facilitated reliable differentiation into all three germ layers and may therefore provide a viable alternative to conventional methods for EB formation.

This new method provided also some insight into how differentiation continues from 2D colonies into 3D aggregates. Immunofluorescence analysis and scRNA-seq data demonstrated that the differential expression in the 2D colonies progresses in 3D aggregates, accompanied by similar segregation of $OCT4^{high}$ and *NODAL*^{high} cells at the outer layer. While the mechanism driving the self-organization may differ between 2D colonies and 3D aggregates, the lack of self-organization of spin-EBs points to the role of pre-organization in 2D colonies in priming the self-segregation of early 3D aggregates. This is also supported by the clear differences in gene expression of μ CP-EBs versus spin-EBs: in the initial aggregates ectodermal genes were higher expressed and after two days also the endodermal and mesodermal differentiation was accelerated. Thus, the spatial 2D organization of confined iPSC colonies seems to progress in the self-detached colonies to provide differentiation advantage in early aggregates. This was accompanied by higher activation of the TGF- β and WNT pathways in early spin-EBs.

In contrast, we did not see clear differences between μ CP-EBs and spin-EBs during directed long-term differentiation toward hematopoietic, mesenchymal, and neuronal lineages. Perhaps the initial divergence in differentiation is equalized over time. In analogy, no significant difference was observed by other authors during directed differentiation of iPSCs obtained from different states of pluripotency to primordial cells [5]. The high inter-donor and inter-experiment variation during long-term differentiation of iPSCs remains a challenge. In the future, a more systematic comparison of different EB-methods and EB-sizes should be performed with much higher sample numbers. Either way, our data demonstrate that μ CP-EBs are clearly capable of differentiation toward hematopoietic, mesenchymal, and neuronal lineages.

5. Conclusion

Spatial self-organization of iPSCs on flat substrates results in radially organized heterogeneity of gene expression, particularly of pluripotency markers. The process seems to be driven by the TGF- β pathway and cell-cell interactions. After detaching from the substrates, self-organization progressed in 3D aggregates. A better understanding of the underlying mechanisms may provide new perspectives for more efficient and directed cellular differentiation. Furthermore, we describe a new scalable method to generate EBs by self-detachment from μ CP substrates, which will be valuable for standardized and automated cell culture regimen.

Author contributions

M.E.M, R.G, G.A, M.Z, and W.W. were involved in conceptualization of research; V-P, and U.S. were involved in the fabrication of PDMS based patterns; M.E.M, G.A, B-Y, K.Z, Z. M, M.A.S.T, O-C, P.G, and S.L. carried out the experiments, M.E.M, L.S, R.L, and I-C participated in scRNA-seq analysis, A.L. provided support for neuronal differentiation,

M.E.M and W.W. wrote the manuscript and all authors contributed and approved the final manuscript.

Data and code availability

Raw data of scRNA-seq and bulk RNA-Seq data are deposited at Gene Expression Omnibus (GEO) under the accession number GSE184604.

Financial Support

Wolfgang Wagner reports financial support was provided by German Research Foundation, Germany. Martin Zenke reports financial support was provided by Federal Ministry of Education and Research Berlin Office. Marcelo A. S. Toledo reports financial support was provided by Alexander von Humboldt Foundation. Wolfgang Wagner is cofounder of Cygenia GmbH. It is a small start up company that can provide service for epigenetic analysis to other researchers. Philipp Glück is also contributing on an hourly basis (and Roman Goetzke was before). Either way, the research described in this manuscript does not address epigenetic analysis and it is not related to the service of Cygenia GmbH.

Declaration of competing interest

The authors declare that they have no known competing financial interests or personal relationships that could have appeared to influence the work reported in this paper.

Acknowledgments

This work was supported by the German Research Foundation (DFG; WA 1706/8–1, WA 1706/11–1, WA 1706/12–1/CRU344, and 363055819/GRK2415), the Interdisciplinary Center for Clinical Research (IZKF) within the faculty of Medicine at the RWTH Aachen University (O3-3), by the Imaging Facility, and the Flow Cytometry Facility, core facilities of the IZKF within the Faculty of Medicine at RWTH Aachen University. This work was supported in part by the Ministry for Innovation, Science and Research of German Federal State of North Rhine-Westphalia, Duesseldorf, Germany (M.Z.) and by the U. Lehmann donation and CAPES-Alexander von Humboldt postdoctoral fellowship (M.A.S.T).

Appendix A. Supplementary data

Supplementary data to this article can be found online at <https://doi.org/10.1016/j.biomaterials.2022.121389>.

References

- M.H. Stewart, M. Bosse, K. Chadwick, P. Menendez, S.C. Bendall, M. Bhatia, Clonal isolation of hESCs reveals heterogeneity within the pluripotent stem cell compartment, *Nat. Methods* 3 (10) (2006) 807–815.
- Q.H. Nguyen, S.W. Lukowski, H.S. Chiu, A. Senabouth, T.J.C. Bruxner, A.N. Christ, N.J. Palpant, J.E. Powell, Single-cell RNA-seq of human induced pluripotent stem cells reveals cellular heterogeneity and cell state transitions between subpopulations, *Genome Res.* 28 (7) (2018) 1053–1066.
- A.M. Singh, T. Hamazaki, K.E. Hankowski, N. Terada, A heterogeneous expression pattern for Nanog in embryonic stem cells, *Stem Cell.* 25 (10) (2007) 2534–2542.
- S.R. Hough, A.L. Laslett, S.B. Grimmond, G. Kolle, M.F. Pera, A continuum of cell states spans pluripotency and lineage commitment in human embryonic stem cells, *PLoS One* 4 (11) (2009), e7708.
- K.X. Lau, E.A. Mason, J. Kie, D.P. De Souza, J. Kloehn, D. Tull, M.J. McConville, A. Keniry, T. Beck, M.E. Blewitt, M.E. Ritchie, S.H. Naik, D. Zalcenstein, O. Korn, S. Su, I.G. Romero, C. Spruce, C.L. Baker, T.C. McGarr, C.A. Wells, M.F. Pera, Unique properties of a subset of human pluripotent stem cells with high capacity for self-renewal, *Nat. Commun.* 11 (1) (2020) 2420.
- S.R. Hough, M. Thornton, E. Mason, J.C. Mar, C.A. Wells, M.F. Pera, Single-cell gene expression profiles define self-renewing, pluripotent, and lineage primed states of human pluripotent stem cells, *Stem Cell Reports* 2 (6) (2014) 881–895.
- A. Warmflash, B. Sorre, F. Etoc, E.D. Siggia, A.H. Brivanlou, A method to recapitulate early embryonic spatial patterning in human embryonic stem cells, *Nat. Methods* 11 (8) (2014) 847–854.
- A. Deglincerti, F. Etoc, M.C. Guerra, I. Martyn, J. Metzger, A. Ruzo, M. Simunovic, A. Yoney, A.H. Brivanlou, E. Siggia, A. Warmflash, Self-organization of human embryonic stem cells on micropatterns, *Nat. Protoc.* 11 (2016) 2223–2232.
- X. Varelas, P. Samavarchi-Tehrani, M. Narimatsu, A. Weiss, K. Cockburn, B. G. Larsen, J. Rossant, J.L. Wrana, The Crumbs complex couples cell density sensing to Hippo-dependent control of the TGF- β -SMAD pathway, *Dev. Cell* 19 (6) (2010) 831–844.
- M. Narimatsu, P. Samavarchi-Tehrani, X. Varelas, J.L. Wrana, Distinct polarity cues direct Taz/Yap and TGF β receptor localization to differentially control TGF β -induced Smad signaling, *Dev. Cell* 32 (5) (2015) 652–656.
- F. Nallet-Staub, X. Yin, C. Gilbert, V. Marsaud, S. Ben Mimoun, D. Javelaud, E. B. Leof, A. Mauviel, Cell density sensing alters TGF- β signaling in a cell-type-specific manner, independent from Hippo pathway activation, *Dev. Cell* 32 (5) (2015) 640–651.
- F. Etoc, J. Metzger, A. Ruzo, C. Kirst, A. Yoney, M.Z. Ozair, A.H. Brivanlou, E. D. Siggia, A balance between secreted inhibitors and edge sensing controls gastruloid self-organization, *Dev. Cell* 39 (3) (2016) 302–315.
- M. Tewary, J. Ostblom, L. Prochazka, T. Zulueta-Coarasa, N. Shakiba, R. Fernandez-Gonzalez, P.W. Zandstra, A stepwise model of reaction-diffusion and positional information governs self-organized human peri-gastrulation-like patterning, *Development* 144 (23) (2017) 4298–4312.
- R. Joshi, P.S. Thakuri, J.C. Buchanan, J. Li, H. Tavana, Microprinted stem cell niches reveal compounding effect of colony size on stromal cells-mediated neural differentiation, *Advanced healthcare materials* 7 (5) (2018) 1700832.
- R. Goetzke, J. Franzen, A. Ostrowska, M. Vogt, A. Blaeser, G. Klein, B. Rath, H. Fischer, M. Zenke, W. Wagner, Does soft really matter? Differentiation of induced pluripotent stem cells into mesenchymal stromal cells is not influenced by soft hydrogels, *Biomaterials* 156 (2017) 147–158.
- S. Sontag, M. Förster, J. Qin, P. Wanek, S. Mitzka, H.M. Schüller, S. Koschmieder, S. Rose-John, K. Seré, M. Zenke, Modelling IRF8 deficient human hematopoiesis and dendritic cell development with engineered iPSC cells, *Stem Cell.* 35 (4) (2017) 898–908.
- M.A.S. Toledo, M. Gatz, S. Sontag, K.V. Gleixner, G. Eisenwort, K. Feldberg, F. Kluge, R. Guareschi, G. Rossetti, A.S. Sechi, O.M.J. Dufva, S.M. Mustjoki, A. Maurer, H.M. Schüller, R. Goetzke, T. Braunschweig, A. Simonowski, J. Panse, M. Jawhar, A. Reiter, F. Hilberg, P. Etmayer, W. Wagner, S. Koschmieder, T. H. Brümmendorf, P. Valent, N. Chatain, M. Zenke, Nintedanib targets KIT D816V neoplastic cells derived from induced pluripotent stem cells of systemic mastocytosis, *Blood* 137 (15) (2021) 2070–2084.
- C.A. Willmann, H. Hameda, L.A. Pieper, M. Lenz, J. Qin, S. Joussen, S. Sontag, P. Wanek, B. Denecke, H.M. Schuler, M. Zenke, W. Wagner, To clone or not to clone? Induced pluripotent stem cells can be generated in bulk culture, *PLoS One* 8 (5) (2013), e65324.
- M. Lenz, R. Goetzke, A. Schenk, C. Schubert, J. Veeck, H. Hameda, S. Koschmieder, M. Zenke, A. Schuppert, W. Wagner, Epigenetic biomarker to support classification into pluripotent and non-pluripotent cells, *Sci. Rep.* 5 (2015) 8973.
- M. Kovarova, B. Koller, Differentiation of mast cells from embryonic stem cells, *Curr. Protoc. Im.* 97 (1) (2012) 22F.10.1–22F.10.16.
- J. Frobel, H. Hameda, M. Lenz, G. Abagnale, S. Joussen, B. Denecke, T. Šarić, M. Zenke, W. Wagner, Epigenetic rejuvenation of mesenchymal stromal cells derived from induced pluripotent stem cells, *Stem cell reports* 3 (3) (2014) 414–422.
- M. Dominici, K. Le Blanc, I. Mueller, I. Slaper-Cortenbach, F. Marini, D. Krause, R. Deans, A. Keating, D. Prockop, E. Horwitz, Minimal criteria for defining multipotent mesenchymal stromal cells, *Intl. Soc. Cell. Therapy posit. statement, Cytotherapy* 8 (4) (2006) 315–317.
- A. Chandrasekaran, H.X. Avci, A. Ochalek, L.N. Rosingh, K. Molnar, L. László, T. Bellák, A. Téglási, K. Pesti, A. Mike, Comparison of 2D and 3D neural induction methods for the generation of neural progenitor cells from human induced pluripotent stem cells, *Stem Cell Res.* 25 (2017) 139–151.
- J.F. Dekkers, M. Alieva, L.M. Wellens, H.C.R. Ariese, P.R. Jamieson, A.M. Vonk, G. D. Amatgaliim, H. Hu, K.C. Oost, H.J.G. Snippert, J.M. Beekman, E.J. Wehrens, J. E. Visvader, H. Clevers, A.C. Rios, High-resolution 3D imaging of fixed and cleared organoids, *Nat. Protoc.* 14 (6) (2019) 1756–1771.
- J. Schindelin, I. Arganda-Carreras, E. Frise, V. Kaynig, M. Longair, T. Pietzsch, S. Preibisch, C. Rueden, S. Saalfeld, B. Schmid, Fiji: an open-source platform for biological-image analysis, *Nat. Methods* 9 (7) (2012) 676–682.
- T. Stuart, A. Butler, P. Hoffman, C. Hafemeister, E. Papalexi, W.M. Mauck III, Y. Hao, M. Stoeckius, P. Smibert, R. Satija, Comprehensive integration of single-cell data, *Cell* 177 (7) (2019) 1888–1902, e21.
- A. McDavid, G. Finak, M. Yajima, MAST: model-based analysis of single cell transcriptomics, *Genome Biol.* 16 (2015) 278.
- G. Yu, L.-G. Wang, Y. Han, Q.-Y. He, clusterProfiler: an R package for comparing biological themes among gene clusters, *OMICS A J. Integr. Biol.* 16 (5) (2012) 284–287.
- M. Nitzan, N. Karaiskos, N. Friedman, N. Rajewsky, Gene expression cartography, *Nature* 576 (7785) (2019) 132–137.
- G. Linderman, J. Zhao, M. Roulis, P. Bielecki, RA Flavell, B. Nadler, Y. Kluger, Zero-preserving imputation of single-cell RNA-seq data, *Nat. Communications* 13 (1) (2022).
- M. Schubert, B. Klinger, M. Klünemann, A. Sieber, F. Uhlitz, S. Sauer, M.J. Garnett, N. Blüthgen, J. Saez-Rodriguez, Perturbation-response genes reveal signaling footprints in cancer gene expression, *Nat. Commun.* 9 (1) (2018) 1–11.
- C.H. Holland, J. Tanevski, J. Perales-Patón, J. Gleixner, M.P. Kumar, E. Mereu, B. A. Joughin, O. Stegle, D.A. Lauffenburger, H. Heyn, Robustness and applicability of

- transcription factor and pathway analysis tools on single-cell RNA-seq data, *Genome Biol.* 21 (1) (2020) 1–19.
- [33] R. Patro, G. Duggal, M.I. Love, R.A. Irizarry, C. Kingsford, Salmon provides fast and bias-aware quantification of transcript expression, *Nat. Methods* 14 (4) (2017) 417–419.
- [34] M.I. Love, W. Huber, S. Anders, Moderated estimation of fold change and dispersion for RNA-seq data with DESeq2, *Genome Biol.* 15 (12) (2014) 1–21.
- [35] F. Haghighi, J. Dahlmann, S. Nakhaei-Rad, A. Lang, I. Kutschka, M. Zenker, G. Kensah, R.P. Piekorz, M.R. Ahmadian, bFGF-mediated pluripotency maintenance in human induced pluripotent stem cells is associated with NRAS-MAPK signaling, *Cell Commun. Signal.* 16 (1) (2018) 1–14.
- [36] L. Sui, L. Bouwens, J.K. Mfopou, Signaling pathways during maintenance and definitive endoderm differentiation of embryonic stem cells, *Int. J. Dev. Biol.* 57 (1) (2013) 1–12.
- [37] A. Totaro, T. Panciera, S. Piccolo, YAP/TAZ upstream signals and downstream responses, *Nat. Cell Biol.* 20 (8) (2018) 888–899.
- [38] G. Abagnale, A. Sechi, M. Steger, Q. Zhou, C.C. Kuo, G. Aydin, C. Schalla, G. Muller-Newen, M. Zenke, I.G. Costa, P. van Rijn, A. Gillner, W. Wagner, Surface topography guides morphology and spatial patterning of induced pluripotent stem cell colonies, *Stem Cell Reports* 9 (2) (2017) 654–666.
- [39] M. Li, J.C. Belmonte, Ground rules of the pluripotency gene regulatory network, *Nat. Rev. Genet.* 18 (3) (2017) 180–191.
- [40] M. Nakanishi, R.R. Mitchell, Y.D. Benoit, L. Orlando, J.C. Reid, K. Shimada, K. C. Davidson, Z. Shapovalova, T.J. Collins, A. Nagy, Human pluripotency is initiated and preserved by a unique subset of founder cells, *Cell* 177 (4) (2019) 910–924, e22.